A Stability Study of some Mixed Finite Elements for Large Deformation Elasticity Problems

F. Auricchio [a,b], L. Beirão da Veiga [c], C. Lovadina [c,b,1] and A. Reali [a,d]

[a] *Dipartimento di Meccanica Strutturale, Università di Pavia, Italy*

[b] *Istituto di Matematica Applicata e Tecnologie Informatiche del CNR, Pavia, Italy*

[c] *Dipartimento di Matematica, Università di Pavia, Italy*

[d] *European School for Advanced Studies in Reduction of Seismic Risk (ROSE School), Università di Pavia, Italy*

Abstract

We consider the finite elasticity problem for incompressible materials, proposing a simple bidimensional problem for which we provide an indication on the solution stability. Furthermore, we study the stability of discrete solutions, obtained by means of some well-known mixed finite elements, and we present several numerical experiments.

Key words: Incompressible Elasticity, Displacement/Pressure formulation, Finite Element Methods, Enhanced Strain Technique, Stability Analysis.

1 Introduction

Nowadays there are several finite element interpolation schemes which perform very well (in terms of accuracy and stability) for the case of small deformation

[1] Corresponding author.
Address: Dipartimento di Matematica, Università di Pavia.
Via Ferrata 1, I-27100, Italy.
Tel.: ++39-0382-505685. Fax: ++39-0382-505602
E-mail: lovadina@dimat.unipv.it

problems, also in the presence of highly constrained situations (i.e. incompressible materials). Examples ranges from standard mixed elements (see, for instance, [4], [7], [9], and the references therein) to enhanced strain elements (see [2], [5], [18], [20] and [24]).

However, it is also well established that the extension of such schemes to the case of finite strain problems is by no way trivial; in particular, even elements which seem to be ideal from a theoretical and a numerical perspective may fail in the large strain range, for example due to the rising of unphysical instabilities for high compression/tension states (see [3], [14], [19] and [26] for more details). It is worth recalling that many interesting strategies have been developed in order to stabilize the methods at hand (cf., for instance, [10], [15] [17], [21], [22] and [23]). However, a satisfactory analysis of finite element methodologies for finite strain problems is still missing.

According to the cited problematics, the present work focuses on a simple finite-strain elastic bidimensional problem for which not only it is possible to compute the solution in closed form but it is also possible to draw some indications on the solution stability for both the continuum and the discrete problems.

After recalling the general finite strain elasticity framework (Section 2), we discuss the proposed 2D continuum problem (Section 3). We then present some possible finite element discretizations of the problem under investigation. In particular, we consider the MINI mixed finite element (see [1]) and the QME mixed-enhanced finite element (see [18]), which have been proved to be stable and well performing in linear elasticity. For both finite elements we are able to present some theoretical considerations on the stability limits of the discrete problems, showing that both formulations fail to reproduce the continuum stability features (Section 4). Finally, we perform extensive numerical simulations to investigate the whole stability range of both finite element discretizations (Section 5).

2 The finite strain incompressible elasticity problem

In this paper we adopt the so-called *material description* to study the finite strain elasticity problem. Accordingly, we suppose that we are given a *reference configuration* $\Omega \subset \mathcal{R}^d$ for a d-dimensional bounded material body $\mathcal{B}$. Therefore, the deformation of $\mathcal{B}$ can be described by means of the map $\hat{\boldsymbol{\varphi}} : \Omega \to \mathcal{R}^d$ defined by

$$\hat{\boldsymbol{\varphi}}(\mathbf{X}) = \mathbf{X} + \hat{\mathbf{u}}(\mathbf{X}) \ , \tag{1}$$

where $\mathbf{X} = (X_1, .., X_d)$ denotes the coordinates of a material point in the reference configuration and $\hat{\mathbf{u}}(\mathbf{X})$ represents the corresponding displacement vector. Following standard notations, (see [6] and [16], for instance) we introduce the deformation gradient $\hat{\mathbf{F}} = \mathbf{F}(\hat{\mathbf{u}})$ and the right Cauchy-Green deformation tensor $\hat{\mathbf{C}} = \mathbf{C}(\hat{\mathbf{u}})$ by setting

$$\hat{\mathbf{F}} = \mathbf{I} + \nabla\hat{\mathbf{u}} \qquad , \qquad \hat{\mathbf{C}} = \hat{\mathbf{F}}^T\hat{\mathbf{F}} \ , \tag{2}$$

where $\mathbf{I}$ is the second-order identity tensor and ∇ is the gradient operator with respect to the coordinates $\mathbf{X}$.

For a homogeneous neo-Hookean material we define (see for example [6] and [8]) the potential energy function as

$$\Psi(\hat{\mathbf{u}}) = \frac{1}{2}\mu\left[\mathbf{I} : \hat{\mathbf{C}} - d\right] - \mu \ln \hat{J} + \frac{\lambda}{2}\,\Theta(\hat{J})^2 \ , \tag{3}$$

where λ and μ are positive constants, " : " represents the usual inner product for second-order tensors and $\hat{J} = \det \hat{\mathbf{F}}$. Moreover, Θ is a real function usually chosen as

$$\Theta(J) = \ln J \qquad \text{or} \qquad \Theta(J) = J - 1 \ . \tag{4}$$

Introducing the pressure-like variable (or simply pressure) $\hat{p} = \lambda\Theta(\hat{J})$, the potential energy (3) can be equivalently written as the following function of $\hat{\mathbf{u}}$ and $\hat{p}$ (still denoted as Ψ with a little abuse of notations)

$$\Psi(\hat{\mathbf{u}}, \hat{p}) = \frac{1}{2}\mu\left[\mathbf{I} : \hat{\mathbf{C}} - d\right] - \mu \ln \hat{J} + \hat{p}\Theta(\hat{J}) - \frac{1}{2\lambda}\hat{p}^2 \ . \tag{5}$$

When the body $\mathcal{B}$ is subjected to a given load $\mathbf{b} = \mathbf{b}(\mathbf{X})$ per unit volume in the reference configuration, the total elastic energy functional reads as follows

$$\Pi(\hat{\mathbf{u}}, \hat{p}) = \int_\Omega \Psi(\hat{\mathbf{u}}, \hat{p}) - \int_\Omega \mathbf{b} \cdot \hat{\mathbf{u}} \ . \tag{6}$$

Therefore, following the Hellinger-Reissner variational principle, equilibrium is derived by searching for critical points of (6) in suitable admissible displacement and pressure spaces $\hat{U}$ and $\hat{P}$. The corresponding Euler-Lagrange equations emanating from (6) lead to solve

$$\begin{cases} \text{Find } (\hat{\mathbf{u}}, \hat{p}) \in \hat{U} \times \hat{P} \text{ such that} \\ \\ \mu \displaystyle\int_\Omega [\hat{\mathbf{F}} - \hat{\mathbf{F}}^{-T}] : \nabla \mathbf{v} + \int_\Omega \hat{p}\, \Theta'(\hat{J}) \hat{J}\, \hat{\mathbf{F}}^{-T} : \nabla \mathbf{v} = \int_\Omega \mathbf{b} \cdot \mathbf{v} \qquad \forall \mathbf{v} \in U \\ \\ \displaystyle\int_\Omega \left(\Theta(\hat{J}) - \frac{\hat{p}}{\lambda} \right) q = 0 \qquad \forall q \in P \ , \end{cases} \tag{7}$$

where U and P are the admissible variation spaces for the displacements and the pressures, respectively. We note that in (7) we used that the linearization of the deformation gradient jacobian is

$$DJ(\hat{\mathbf{u}})[\mathbf{v}] = J(\hat{\mathbf{u}}) \mathbf{F}(\hat{\mathbf{u}})^{-T} : \nabla \mathbf{v} = \hat{J}\, \hat{\mathbf{F}}^{-T} : \nabla \mathbf{v} \qquad \forall \mathbf{v} \in U \ . \tag{8}$$

Without loss of generality, from now on we select $\Theta(J) = \ln J$ (see (4)). Moreover, we focus on the case of an *incompressible* material, which corresponds to take the limit $\lambda \to +\infty$ in (7). Therefore, our problem becomes

$$\begin{cases} \text{Find } (\hat{\mathbf{u}}, \hat{p}) \in \hat{U} \times \hat{P} \text{ such that} \\ \\ \mu \displaystyle\int_\Omega \hat{\mathbf{F}} : \nabla \mathbf{v} + \int_\Omega (\hat{p} - \mu) \hat{\mathbf{F}}^{-T} : \nabla \mathbf{v} - \int_\Omega \mathbf{b} \cdot \mathbf{v} = \mathbf{0} \qquad \forall \mathbf{v} \in U \\ \\ \displaystyle\int_\Omega q\ \ln \hat{J} = 0 \qquad \forall q \in P \ , \end{cases} \tag{9}$$

or, in residual form,

$$\begin{cases} \text{Find } (\hat{\mathbf{u}}, \hat{p}) \in \hat{U} \times \hat{P} \text{ such that} \\ \\ \mathcal{R}_u((\hat{\mathbf{u}}, \hat{p}), \mathbf{v}) = \mathbf{0} \qquad \forall \mathbf{v} \in U \\ \\ \mathcal{R}_p((\hat{\mathbf{u}}, \hat{p}), q) = 0 \qquad \forall q \in P \ , \end{cases} \tag{10}$$

where

$$\begin{cases} \mathcal{R}_u((\hat{\mathbf{u}}, \hat{p}), \mathbf{v}) := \mu \displaystyle\int_\Omega \hat{\mathbf{F}} : \nabla \mathbf{v} + \int_\Omega (\hat{p} - \mu) \hat{\mathbf{F}}^{-T} : \nabla \mathbf{v} - \int_\Omega \mathbf{b} \cdot \mathbf{v} \\ \\ \mathcal{R}_p((\hat{\mathbf{u}}, \hat{p}), q) := \displaystyle\int_\Omega q\ \ln \hat{J} \ . \end{cases} \tag{11}$$

We now derive the linearization of problem (9) around a generic point $(\hat{\mathbf{u}}, \hat{p})$. Observing that

$$D\hat{\mathbf{F}}^{-T}(\hat{\mathbf{u}})[\mathbf{u}] = -\hat{\mathbf{F}}^{-T}(\nabla \mathbf{u})^T \hat{\mathbf{F}}^{-T} \qquad \forall \mathbf{u} \in U \ , \tag{12}$$

we easily get the problem for the *infinitesimal* increment $(\mathbf{u}, p)$

$$\begin{cases} \text{Find } (\mathbf{u}, p) \in U \times P \text{ such that} \\ \\ \mu \displaystyle\int_\Omega \nabla \mathbf{u} : \nabla \mathbf{v} + \int_\Omega (\mu - \hat{p})(\hat{\mathbf{F}}^{-1}\nabla \mathbf{u})^T : \hat{\mathbf{F}}^{-1}\nabla \mathbf{v} \\ \\ \qquad + \displaystyle\int_\Omega p\hat{\mathbf{F}}^{-T} : \nabla \mathbf{v} = -\mathcal{R}_u((\hat{\mathbf{u}}, \hat{p}), \mathbf{v}) \qquad \forall \mathbf{v} \in U \\ \\ \displaystyle\int_\Omega q\hat{\mathbf{F}}^{-T} : \nabla \mathbf{u} = -\mathcal{R}_p((\hat{\mathbf{u}}, \hat{p}), q) \qquad \forall q \in P \ . \end{cases} \tag{13}$$

Remark 1 *Since problem* (13) *is the linearization of problem* (9) *(or equivalently* (10)*), it can be interpreted as the generic step of a Newton-like iteration procedure for the solution of the non-linear problem* (9)*.*

Remark 2 *Taking* $(\hat{\mathbf{u}}, \hat{p}) = (0, 0)$ *in (13), we immediately recover the classical linear incompressible elasticity problem for small deformations, i.e.*

$$\begin{cases} \text{Find } (\mathbf{u}, p) \in U \times P \text{ such that} \\ \\ 2\mu \displaystyle\int_\Omega \boldsymbol{\varepsilon}(\mathbf{u}) : \boldsymbol{\varepsilon}(\mathbf{v}) + \int_\Omega p \ \mathrm{div}\, \mathbf{v} = \int_\Omega \mathbf{b} \cdot \mathbf{v} \qquad \forall \mathbf{v} \in U \\ \\ \displaystyle\int_\Omega q \ \mathrm{div}\, \mathbf{u} = 0 \qquad \forall q \in P \ , \end{cases} \tag{14}$$

where $\boldsymbol{\varepsilon}(\cdot)$ *denotes the symmetric gradient operator.*

3 A model problem for finite strain incompressible elasticity

In this section we present a *simple* bidimensional problem which nonetheless shows some of the difficulties arising in general nonlinear elastic problems for incompressible materials.

Using the usual Cartesian coordinates (X, Y), we consider a square material

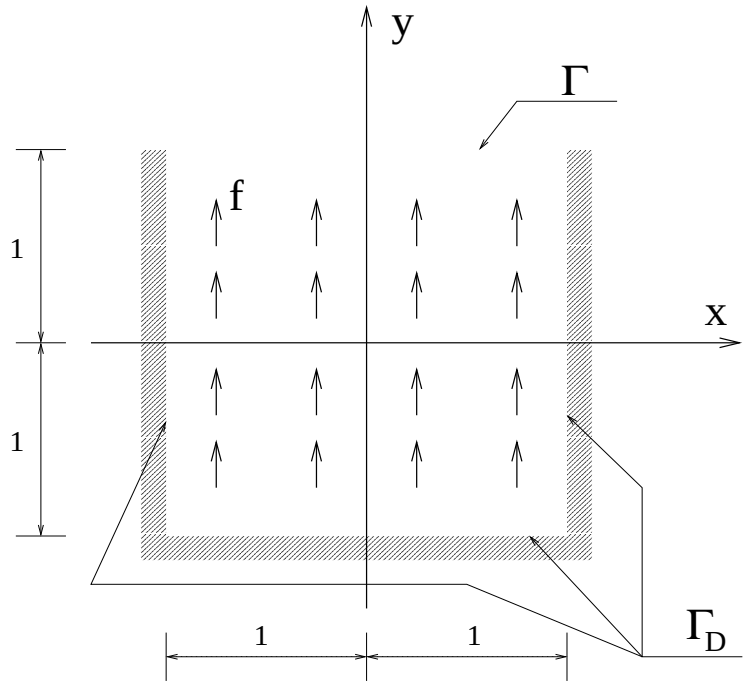

Fig. 1. Problem domain Ω.

body whose reference configuration is $\Omega = (-1,1) \times (-1,1)$; we denote with $\Gamma = [-1,1] \times \{1\}$ the upper part of its boundary, while the remaining part of $\partial\Omega$ is denoted with Γ_D (cf. Fig. 1). The body Ω is clamped along Γ_D and subjected to the volume force $\mathbf{b} = \gamma\mathbf{f}$, where $\mathbf{f} = (0,1)^T$ and γ is a real parameter.

Therefore, the equilibrium problem leads to solve the following variational system (see (9))

$$\begin{cases} \text{Find } (\hat{\mathbf{u}}, \hat{p}) \in \hat{U} \times \hat{P} \text{ such that} \\ \\ \mu \displaystyle\int_\Omega \hat{\mathbf{F}} : \nabla\mathbf{v} + \int_\Omega (\hat{p} - \mu)\hat{\mathbf{F}}^{-T} : \nabla\mathbf{v} = \gamma \int_\Omega \mathbf{f} \cdot \mathbf{v} \qquad \forall \mathbf{v} \in U \\ \\ \displaystyle\int_\Omega q \, \ln \hat{J} = 0 \qquad \forall q \in P \, . \end{cases} \tag{15}$$

It is not our intention to rigorously specify the regularity needed for the space involved in the variational formulation (15), and we refer to [11] and [12] for details on such a point. Instead, we wish to notice that system (15) constitutes a set of *nonlinear* equations for which a trivial solution can be easily found *for every* $\gamma \in \mathbf{R}$, i.e. $(\hat{\mathbf{u}}, \hat{p}) = (\mathbf{0}, \gamma r)$, where $r = r(X,Y) = 1 - Y$.

Remark 3 *We are not claiming that, for each* $\gamma \in \mathbf{R}$, $(\hat{\mathbf{u}}, \hat{p}) = (\mathbf{0}, \gamma r)$ *is the only solution of the system.*

Whenever an incremental loading procedure is considered, the passage from γ to $\gamma + \Delta\gamma$ in (15) is typically solved by a Newton's technique. Supposing that at γ convergence has been reached, the first iteration step of Newton's method with initial guess $(\hat{\mathbf{u}}, \hat{p}) = (\mathbf{0}, \gamma r)$ consists (recalling the linearized problem (13)) in solving

$$\begin{cases} \text{Find } (\mathbf{u}, p) \in U \times P \text{ such that} \\ \\ 2\mu \displaystyle\int_\Omega \boldsymbol{\varepsilon}(\mathbf{u}) : \boldsymbol{\varepsilon}(\mathbf{v}) - \gamma \int_\Omega r (\nabla \mathbf{u})^T : \nabla \mathbf{v} + \int_\Omega p \, \mathrm{div}\, \mathbf{v} = \Delta\gamma \int_\Omega \mathbf{f} \cdot \mathbf{v} \\ \\ \displaystyle\int_\Omega q \, \mathrm{div}\, \mathbf{u} = 0 \ , \end{cases} \tag{16}$$

for every $(\mathbf{v}, q) \in U \times P$. Letting

$$U = \left\{ \mathbf{v} \in H^1(\Omega)^2 \ : \ \mathbf{v}_{|\Gamma_D} = 0 \right\} \ ; \qquad P = L^2(\Omega) \ , \tag{17}$$

we consider system (16) as a *model problem* for our subsequent considerations. This means that from now on in this Section we study the linear problem (16) with the hope that this may give some indications on the more general non-linear problem (15).

Denoting with $\mathbf{A}^S$ the symmetric part of a generic second-order tensor $\mathbf{A}$ and introducing the bilinear forms

$$a_\gamma(\mathbf{F}, \mathbf{G}) =: 2\mu \int_\Omega \mathbf{F}^S : \mathbf{G}^S - \gamma \int_\Omega r \, \mathbf{F}^T : \mathbf{G} \tag{18}$$

$$b(\mathbf{v}, q) =: \int_\Omega q \ \mathrm{div}\, \mathbf{v} \ , \tag{19}$$

problem (16) can be written as

$$\begin{cases} \text{Find } (\mathbf{u}, p) \in U \times P \text{ such that} \\ \\ a_\gamma(\nabla \mathbf{u}, \nabla \mathbf{v}) + b(\mathbf{v}, p) = \Delta\gamma \displaystyle\int_\Omega \mathbf{f} \cdot \mathbf{v} \qquad \forall \mathbf{v} \in U \\ \\ b(\mathbf{u}, q) = 0 \qquad\qquad \forall q \in P \ . \end{cases} \tag{20}$$

Therefore, we are clearly facing a typical (parameter-depending) saddle-point

problem. As it is well-established (cf. [7]), the crucial properties for the well-posedness are, together with continuity:

- *the inf-sup condition*, i.e. the existence a positive constant β such that

$$\inf_{q\in P}\sup_{\mathbf{v}\in U}\frac{b(\mathbf{v},q)}{||\mathbf{v}||_U||q||_P}\geq\beta\ ; \tag{21}$$

- *the invertibility on the kernel condition*, i.e. the existence a positive constant $\alpha(\gamma,\mu)$ such that

$$\inf_{\mathbf{v}\in Ker\,B}\sup_{\mathbf{u}\in Ker\,B}\frac{a_\gamma(\nabla\mathbf{u},\nabla\mathbf{v})}{||\mathbf{u}||_U||\mathbf{v}||_U}\geq\alpha(\gamma,\mu)\ , \tag{22}$$

  where

$$Ker\,B=\{\mathbf{v}\in U\ :\ b(\mathbf{v},q)=0\qquad\forall q\in P\}\ . \tag{23}$$

As far as the inf-sup condition is concerned, it is a classical result that it holds for the divergence operator. We therefore focus our attention on condition (22). In particular, we will show that the form $a_\gamma(\cdot,\cdot)$ is *coercive* on $Ker\,B$ whenever γ stays in a suitable range of values. We thus expect that within such a range of γ, the trivial solution $(\hat{\mathbf{u}},\hat{p})=(\mathbf{0},\gamma r)$ is unique and stable for the *continuous* problem.

3.1 The stability range

We now investigate on the coercivity on $Ker\,B$ of $a_\gamma(\cdot,\cdot)$. More precisely, recalling the well-known Korn's inequality, we search for conditions on γ implying the existence of a constant $c(\gamma,\mu)>0$ such that

$$2\mu\int_\Omega|\boldsymbol{\varepsilon}(\mathbf{v})|^2-\gamma\int_\Omega r\,(\nabla\mathbf{v})^T:\nabla\mathbf{v}\geq c(\gamma,\mu)\int_\Omega|\boldsymbol{\varepsilon}(\mathbf{v})|^2\qquad\forall\mathbf{v}\in Ker\,B\ . \tag{24}$$

Since $\mathrm{div}(\nabla\mathbf{v})^T=\mathbf{0}$ for every divergence-free function $\mathbf{v}$ (i.e. for every $\mathbf{v}\in Ker\,B$), an integration by parts gives

$$2\mu\int_\Omega|\boldsymbol{\varepsilon}(\mathbf{v})|^2-\gamma\int_\Omega r\,(\nabla\mathbf{v})^T:\nabla\mathbf{v}=2\mu\int_\Omega|\boldsymbol{\varepsilon}(\mathbf{v})|^2+\gamma\int_\Omega\nabla\,r\cdot[\nabla\mathbf{v}]\mathbf{v}\ . \tag{25}$$

Above, the boundary integral arising from integration by parts disappears because of the boundary conditions on $\mathbf{v}$, and because on Γ the function $r=1-Y$ vanishes.

Now, a further integration by parts leads to

$$\gamma \int_\Omega \nabla r \cdot [\nabla \mathbf{v}]\mathbf{v} = \gamma \left(- \int_\Omega H(r)\mathbf{v}\cdot\mathbf{v} + \int_\Gamma (\mathbf{v}\cdot\nabla r)(\mathbf{v}\cdot\mathbf{n}) \right) , \qquad (26)$$

where $\mathbf{n}$ is the outward normal vector and $H(r)$ is the Hessian matrix of the function r. But $r = 1 - Y$ is linear, hence $H(r) = 0$. On the other hand, on the boundary Γ we have $\nabla r = -\mathbf{n}$, hence we deduce that

$$\gamma \int_\Omega \nabla r \cdot \, [\nabla \mathbf{v}]\mathbf{v} = -\gamma \int_\Gamma (\mathbf{v}\cdot\mathbf{n})^2 \ . \qquad (27)$$

From (24), (25) and (27) we conclude that our form $a_\gamma(\cdot,\cdot)$ will be coercive on $Ker\, B$ if there exists a constant $c(\gamma,\mu) > 0$ such that

$$2\mu \int_\Omega |\boldsymbol{\varepsilon}(\mathbf{v})|^2 - \gamma \int_\Gamma (\mathbf{v}\cdot\mathbf{n})^2 \geq c(\gamma,\mu) \int_\Omega |\boldsymbol{\varepsilon}(\mathbf{v})|^2 \qquad \forall \mathbf{v} \in Ker\, B \ . \qquad (28)$$

By (28) we first infer that for $\gamma \leq 0$ we can simply take $c(\gamma,\mu) = 2\mu$. Furthermore, setting

$$\alpha_M = \sup_{\mathbf{v}\in Ker\, B} \frac{\displaystyle\int_\Gamma (\mathbf{v}\cdot\mathbf{n})^2}{\displaystyle\int_\Omega |\boldsymbol{\varepsilon}(\mathbf{v})|^2} > 0 \ , \qquad (29)$$

we see that condition (28) still holds whenever

$$\gamma < \frac{2\mu}{\alpha_M} \ . \qquad (30)$$

Remark 4 *We remark that condition (28) cannot hold for arbitrarily large positive values of* γ. *Indeed, let* $\mathbf{w}$ *be a function in* $KerB$ *which does not vanish on* Γ. *Hence*

$$\int_\Gamma (\mathbf{w}\cdot\mathbf{n})^2 > 0.$$

Choosing γ^* *as*

$$\gamma^* := \frac{2\mu \displaystyle\int_\Omega |\boldsymbol{\varepsilon}(\mathbf{w})|^2}{\displaystyle\int_\Gamma (\mathbf{w}\cdot\mathbf{n})^2} \ , \qquad (31)$$

it follows that

$$2\mu \int_\Omega |\boldsymbol{\varepsilon}(\mathbf{w})|^2 - \gamma \int_\Gamma (\mathbf{w}\cdot\mathbf{n})^2 \le 0 \tag{32}$$

for all $\gamma \ge \gamma^*$. As a consequence, coercivity on the kernel surely fails for sufficiently large positive values of γ.

We now give an estimate of α_M by establishing the following Proposition.

Proposition 5 *Suppose that $\Omega = (-1,1)\times(-1,1)$. Then $\alpha_M \le 2/3$.*

Proof. Take $\mathbf{v} = (v_1, v_2) \in (Ker\, B) \cap C^1(\bar\Omega)$ and observe that on Γ we have $\mathbf{v}\cdot\mathbf{n} = v_2$. Therefore

$$\int_\Gamma (\mathbf{v}\cdot\mathbf{n})^2 = \int_\Gamma |v_2|^2. \tag{33}$$

Since for every $X \in [-1,1]$ it holds $v_2(X,-1) = 0$, we get

$$v_2(X,1) = \int_{-1}^{1} v_{2,Y}(X,Y)dY \ .$$

Hence, the Cauchy-Schwarz inequality gives

$$\int_\Gamma |v_2|^2 \le 2\int_\Omega |v_{2,Y}|^2 \ . \tag{34}$$

Using $\operatorname{div}\mathbf{v} = 0$, we obtain

$$\int_\Gamma |v_2|^2 \le \int_\Omega |v_{1,X}|^2 + \int_\Omega |v_{2,Y}|^2 \le \int_\Omega |\ \varepsilon_{11}(\mathbf{v})\ |^2 + \int_\Omega |\ \varepsilon_{22}(\mathbf{v})\ |^2 \tag{35}$$

for all $\mathbf{v} \in (Ker\, B) \cap C^1(\bar\Omega)$.

Before proceeding, we need to introduce some notation. For every point $P = (X,1)$ with $X \in [-1,1]$, we define the oriented rectilinear path from point P^1_X to point P (see Fig. 2), parametrized by

$$\boldsymbol{\gamma}^1_X(s) = (-1 + s/\sqrt{2}, -X + s/\sqrt{2}) \qquad s \in [0, \sqrt{2}(X+1)] \ , \tag{36}$$

and with unit tangent vector

$$\boldsymbol{\tau}_1 = (1/\sqrt{2}, 1/\sqrt{2}) \ . \tag{37}$$

Similarly, for every $X \in [-1,1]$, we define the oriented rectilinear path from point P^2_X to point P (see Fig. 2), parametrized by

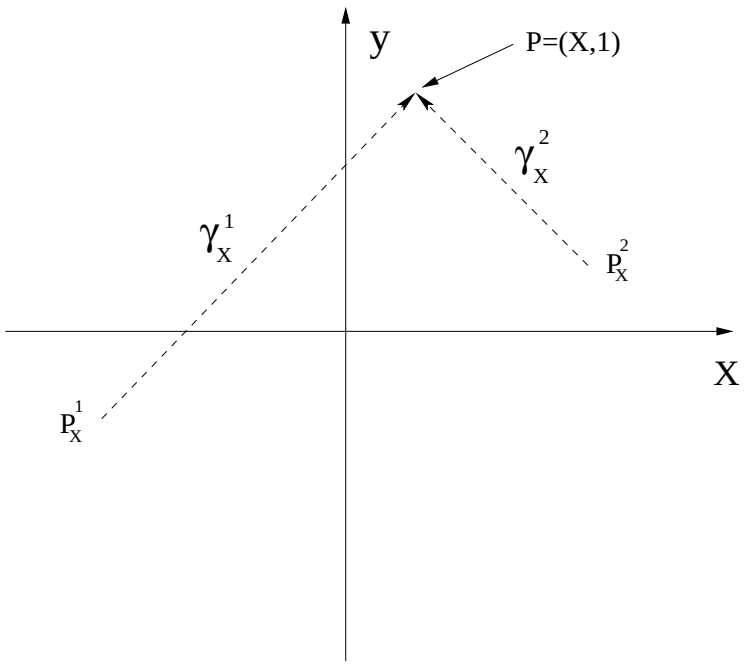

Fig. 2. Oriented paths $\boldsymbol{\gamma}_X^1$ and $\boldsymbol{\gamma}_X^2$ on Ω.

$$\boldsymbol{\gamma}_X^2(s) = (1 - s/\sqrt{2}, X + s/\sqrt{2}) \qquad s \in [0, \sqrt{2}(1 - X)] \ , \tag{38}$$

and with unit tangent vector

$$\boldsymbol{\tau}_2 = (-1/\sqrt{2}, 1/\sqrt{2}) \ . \tag{39}$$

Moreover, we introduce the union path $\boldsymbol{\gamma}_X = \boldsymbol{\gamma}_X^1 \cup \{-\boldsymbol{\gamma}_X^2\}$ going from point P_X^1 to point P_X^2.

For all $X \in [-1, 1]$, it clearly holds

$$v_2(X, 1) = \frac{1}{\sqrt{2}} \mathbf{v}(X, 1) \cdot \boldsymbol{\tau}_1 + \frac{1}{\sqrt{2}} \mathbf{v}(X, 1) \cdot \boldsymbol{\tau}_2 \ . \tag{40}$$

Observing that $\mathbf{v}$ vanishes on $\{-1\} \times [-1, 1]$ and integrating along $\boldsymbol{\gamma}_X^1$, the first term in the right-hand side of (40) can be written as

$$\mathbf{v}(X, 1) \cdot \boldsymbol{\tau}_1 = \int_0^{\sqrt{2}(X+1)} \nabla(\mathbf{v} \cdot \boldsymbol{\tau}_1)(\boldsymbol{\gamma}_X^1(s)) \cdot \boldsymbol{\tau}_1 \, \mathrm{d}s \ , \tag{41}$$

which, after some simple algebra, gives

$$\mathbf{v}(X,1)\cdot\boldsymbol{\tau}_1=\int_0^{\sqrt{2}(X+1)}\boldsymbol{\varepsilon}\Big(\mathbf{v}(\boldsymbol{\gamma}_X^1(s))\Big)\boldsymbol{\tau}_1\cdot\boldsymbol{\tau}_1\,\mathrm{d}s\ . \tag{42}$$

Recalling that $\operatorname{div}\mathbf{v}=0$, it is easy to see that in Ω we have

$$\boldsymbol{\varepsilon}(\mathbf{v})\boldsymbol{\tau}_1\cdot\boldsymbol{\tau}_1=\varepsilon_{12}(\mathbf{v})\ . \tag{43}$$

Using (43) and (42), we obtain

$$\mathbf{v}(X,1)\cdot\boldsymbol{\tau}_1=\int_0^{\sqrt{2}(X+1)}\varepsilon_{12}(\boldsymbol{\gamma}_X^1(s))\,\mathrm{d}s\ , \tag{44}$$

or, in more compact form,

$$\mathbf{v}(X,1)\cdot\boldsymbol{\tau}_1=\int_{\boldsymbol{\gamma}_X^1}\varepsilon_{12}(\mathbf{v})\ . \tag{45}$$

Treating similarly the second term in the right-hand side of (40), but using the path $\boldsymbol{\gamma}_X^2$, it can be shown that

$$\mathbf{v}(X,1)\cdot\boldsymbol{\tau}_2=-\int_{\boldsymbol{\gamma}_X^2}\varepsilon_{12}(\mathbf{v})\ . \tag{46}$$

Recalling (40), from (45) (46) we get

$$v_2(X,1)=\frac{1}{\sqrt{2}}\Big(\int_{\boldsymbol{\gamma}_X^1}\varepsilon_{12}(\mathbf{v})-\int_{\boldsymbol{\gamma}_X^2}\varepsilon_{12}(\mathbf{v})\Big)=\frac{1}{\sqrt{2}}\int_{\boldsymbol{\gamma}_X}\varepsilon_{12}(\mathbf{v})\ , \tag{47}$$

so that we obtain

$$\int_\Gamma\mid v_2\mid^2=\int_{-1}^1\mid v_2(X,1)\mid^2\ \mathrm{d}X=\frac{1}{2}\int_{-1}^1\left|\int_{\boldsymbol{\gamma}_X}\varepsilon_{12}(\mathbf{v})\right|^2\ \mathrm{d}X\ . \tag{48}$$

From (48) and observing that $\mid\boldsymbol{\gamma}_X^1\mid+\mid\boldsymbol{\gamma}_X^2\mid=2\sqrt{2}$ for all $X\in[-1,1]$, the Cauchy-Schwarz inequality yields

$$\int_\Gamma\mid v_2\mid^2\leq\sqrt{2}\int_{-1}^1\Big(\int_{\boldsymbol{\gamma}_X}\mid\varepsilon_{12}(\mathbf{v})\mid^2\Big)\,\mathrm{d}X\ . \tag{49}$$

Setting

$$\Omega_1=\Big\{(X,Y)\in\Omega\ :\ Y\geq X\Big\}\qquad\Omega_2=\Big\{(X,Y)\in\Omega\ :\ Y\geq -X\Big\}\ , \tag{50}$$

we easily get, using a simple change of variables,

$$\int_{-1}^{1}\int_{\boldsymbol{\gamma}_X^1} \mid \varepsilon_{12}(\mathbf{v}) \mid^2 = \sqrt{2}\int_{\Omega_1} \mid \varepsilon_{12}(\mathbf{v}) \mid^2 \leq \sqrt{2}\int_{\Omega} \mid \varepsilon_{12}(\mathbf{v}) \mid^2 , \tag{51}$$

and

$$\int_{-1}^{1}\int_{\boldsymbol{\gamma}_X^2} \mid \varepsilon_{12}(\mathbf{v}) \mid^2 = \sqrt{2}\int_{\Omega_2} \mid \varepsilon_{12}(\mathbf{v}) \mid^2 \leq \sqrt{2}\int_{\Omega} \mid \varepsilon_{12}(\mathbf{v}) \mid^2 \ . \tag{52}$$

From (49), splitting the integral on $\boldsymbol{\gamma}_X$ into the contributions on $\boldsymbol{\gamma}_X^1$ and $\boldsymbol{\gamma}_X^2$, using bounds (51)-(52) we obtain

$$\int_{\Gamma} \mid v_2 \mid^2 \leq 4\int_{\Omega} \mid \varepsilon_{12}(\mathbf{v}) \mid^2 \ . \tag{53}$$

Recalling (33), from (35) and (53) it follows

$$\int_{\Gamma} |\mathbf{v}\cdot\mathbf{n}|^2 \leq \frac{2}{3}\int_{\Omega} \mid \boldsymbol{\varepsilon}(\mathbf{v}) \mid^2 \tag{54}$$

for all $\mathbf{v} \in (Ker\, B) \cap C^1(\bar{\Omega})$.

By density the same estimate holds in $Ker\, B$, so that

$$\alpha_M = \sup_{\mathbf{v}\in Ker\, B} \frac{\displaystyle\int_{\Gamma}(\mathbf{v}\cdot\mathbf{n})^2}{\displaystyle\int_{\Omega}|\boldsymbol{\varepsilon}(\mathbf{v})|^2} \leq \frac{2}{3} , \tag{55}$$

which concludes the proof. □

Remark 6 *We remark that the above estimate of α_M is not guaranteed to be sharp. However, it is sufficient for our subsequent considerations.*

To summarize, our analysis shows that the linearized *continuous* problem (16) is well-posed and *positive-definite* on the relevant kernel $Ker\, B$ if

$$\gamma \in \Big(-\infty, \frac{2\mu}{\alpha_M}\Big) \supseteq (-\infty, 3\mu) \ . \tag{56}$$

4 Discrete stability range: some theoretical results

The goal of the present Section is to investigate the possibility of solving the non-linear problem presented in Section 3 through a finite element discretiza-

tion. Since the first step of an iterative procedure for the solution of non-linear problem (15) coincides with the infinitesimal strain problem, we concentrate our attention on discretizations which are at least stable in such a regime. This can be accomplished by considering finite element methods satisfying the discrete *inf-sup* condition, as the ones studied in this Section.

We recall that the continuous linearized problems (16) are surely stable, in the sense that both the *inf-sup* and the *coercivity on the kernel* conditions hold true, whenever the parameter γ satisfies

$$-\infty < \gamma < 3\mu \ . \tag{57}$$

On the other hand, the continuous linearized problems (16) become unstable for suitable large values of γ (cf. Remark 4). We point out that this lack of stability is only addressed to a failure of the *coercivity on the kernel* condition. Indeed, for the proposed problem the *inf-sup* condition is *independent* of γ, and therefore it is the same one required for the small deformation framework.

Since a reliable numerical approximation should be able to correctly reproduce the stability properties of the continuous problem, the discussion above highlights the importance of studying whether or not a given finite element method satisfies a discrete *coercivity on the kernel* condition, at least for γ in the range shown by (57). With this respect, we consider the MINI element (cf. [1]) and the QME element (cf. [18]), rigorously proving that their stability range are somehow quite different from the continuous problem one. However, we point out that our theoretical analysis is far from being *complete*, although in accordance with the numerical tests presented in Section 5.

4.1 The MINI element

We now consider the discretized counterpart of problem (16), using the MINI element (cf. [1]).

Let $\mathcal{T}_h$ be a triangular mesh of Ω, h being the meshsize. For the discretization of the displacement field, we take

$$U_h = \left\{ \mathbf{v}_h \in U \ : \ \mathbf{v}_{h|T} \in \mathcal{P}_1(T)^2 + \mathcal{B}(T)^2 \qquad \forall T \in \mathcal{T}_h \right\} \ , \tag{58}$$

where $\mathcal{P}_1(T)$ is the space of linear functions on T, and $\mathcal{B}(T)$ is the linear space generated by b_T, the standard cubic bubble function on T. For the pressure discretization, we take

$$P_h = \left\{ q_h \in H^1(\Omega) \ : \ q_{h|T} \in \mathcal{P}_1(T) \qquad \forall T \in \mathcal{T}_h \right\} \ . \tag{59}$$

Therefore, the discretization of problem (16) reads as follows.

Find $(\mathbf{u}_h; p_h) \in U_h \times P_h$ such that:

$$\begin{cases} 2\mu \int_\Omega \boldsymbol{\varepsilon}(\mathbf{u}_h) : \boldsymbol{\varepsilon}(\mathbf{v}_h) - \gamma \int_\Omega r \, (\nabla \mathbf{u}_h)^T : \nabla \mathbf{v}_h \\ \qquad\qquad + \int_\Omega p_h \ \mathrm{div}\, \mathbf{v}_h = \Delta\gamma \int_\Omega \mathbf{f} \cdot \mathbf{v}_h \qquad \forall \mathbf{v}_h \in U_h \\ \int_\Omega q_h \, \mathrm{div}\, \mathbf{u}_h = 0 \qquad\qquad \forall q_h \in P_h \ . \end{cases} \tag{60}$$

Introducing the discrete kernel as

$$K_h = \left\{ \mathbf{v}_h \in U_h \ : \ \int_\Omega q_h \, \mathrm{div}\, \mathbf{u}_h = 0 \qquad \forall q_h \in P_h \right\} \ , \tag{61}$$

we are interested in analyzing for which γ there exists a constant $c_M(\gamma, \mu) > 0$ such that

$$a_\gamma(\nabla \mathbf{v}_h, \nabla \mathbf{v}_h) \geq c_M(\gamma, \mu) \int_\Omega \mid \boldsymbol{\varepsilon}(\mathbf{v}_h) \mid^2 \qquad \forall \mathbf{v}_h \in K_h \ , \tag{62}$$

where

$$a_\gamma(\nabla \mathbf{v}_h, \nabla \mathbf{v}_h) := 2\mu \int_\Omega \boldsymbol{\varepsilon}(\mathbf{v}_h) : \boldsymbol{\varepsilon}(\mathbf{v}_h) - \gamma \int_\Omega r \, (\nabla \mathbf{v}_h)^T : \nabla \mathbf{v}_h \ . \tag{63}$$

We develop our analysis considering the meshes used for the numerical tests presented in Section 5. Therefore $\mathcal{T}_h$ is built by squares of side $2h$, each divided into eight triangles according with the pattern shown in Fig. 3.

We have the following result.

Proposition 7 *For problem (60), the discrete coercivity on the kernel condition (62) does not hold, whenever $\gamma > 3\mu/2$.*

Proof. Take any two adjacent triangles T_1 and T_2, both with a side contained in $[-1, 1] \times \{-1\}$ (see Fig. 3). Consider the function $\mathbf{w}_h = (w_1, w_2) \in U_h$ defined as

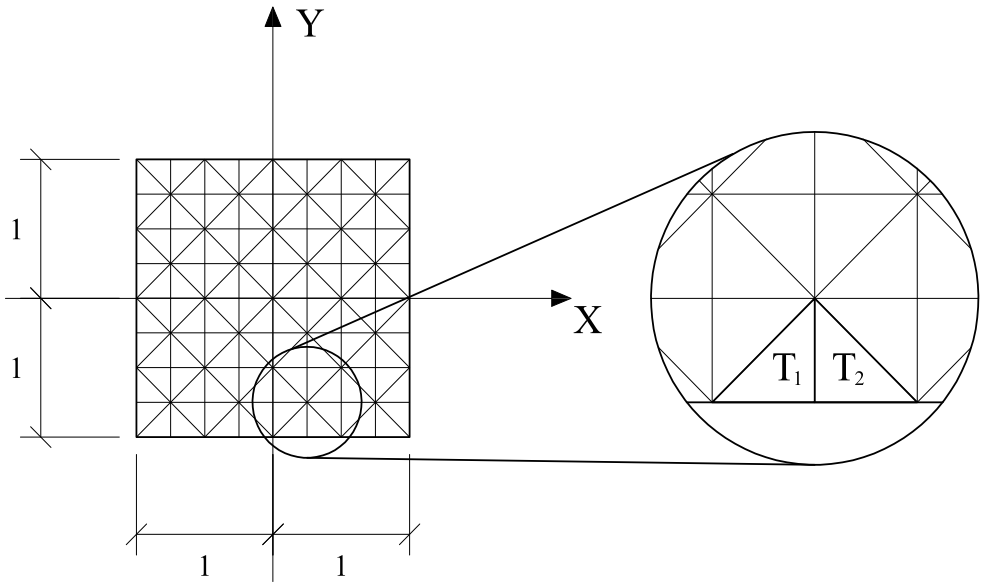

Fig. 3. Triangular mesh for the MINI element.

$$w_1 = 0 \qquad ; \qquad w_2 = \begin{cases} b_{T_1} & \text{on } T_1 \\ -b_{T_2} & \text{on } T_2 \\ 0 & \text{otherwise .} \end{cases} \tag{64}$$

It is easy to see that

$$\int_\Omega q_h \,\mathrm{div}\, \mathbf{w}_h = \int_{T_1 \cup T_2} q_h \,\mathrm{div}\, \mathbf{w}_h = -\int_{T_1 \cup T_2} \nabla q_h \cdot \mathbf{w}_h = 0 \qquad \forall q_h \in P_h \ , \tag{65}$$

so that $\mathbf{w}_h \in K_h$. From (63) and (64), we get

$$a_\gamma(\mathbf{w}_h, \mathbf{w}_h) = 2\mu \int_{T_1 \cup T_2} \left[(w_{2,Y})^2 + \frac{1}{2}(w_{2,X})^2 \right] - \gamma \int_{T_1 \cup T_2} (1 - Y)\,(w_{2,Y})^2 \ . \tag{66}$$

Using that for our particular mesh it holds

$$\int_T (b_{T,Y})^2 = \int_T (b_{T,X})^2 \qquad \forall T \in \mathfrak{T}_h \ , \tag{67}$$

and noting that on $T_1 \cup T_2$ we obviously have $Y < h - 1$, from (64) and (66) it follows

$$a_\gamma(\mathbf{w}, \mathbf{w}) \leq \Big(3\mu - (2-h)\gamma\Big) \int_{T_1 \cup T_2} (w_{2,Y})^2 \ . \tag{68}$$

Therefore the form $a_\gamma(\cdot, \cdot)$ fails to be coercive on K_h whenever γ and h are such that

$$3\mu - (2-h)\gamma \leq 0 \ . \tag{69}$$

It follows that, for $\gamma > 3\mu/2$, the coercivity on the kernel breaks down, provided h is sufficiently small. $\square$

We now prove the following Proposition.

Proposition 8 *For problem (60), the discrete coercivity on the kernel condition (62) is satisfied, independently of the meshsize, whenever $\gamma < \mu$.*

Proof. It is easy to check that, for $-\mu < \gamma < \mu$ and $-1 < Y < 1$, there exists a constant $c > 0$ such that

$$2\mu \mathbf{A}^S : \mathbf{A}^S - \gamma r \mathbf{A}^T : \mathbf{A} \ \geq \ c \mid \mathbf{A}^S \mid^2 \tag{70}$$

for every second order tensor $\mathbf{A}$. From the pointwise positivity property (70) it easily follows that, for $-\mu < \gamma < \mu$, the bilinear form (see (63))

$$a_\gamma(\nabla \mathbf{u}, \nabla \mathbf{v}) = 2\mu \int_\Omega \boldsymbol{\varepsilon}(\mathbf{u}) : \boldsymbol{\varepsilon}(\mathbf{v}) - \gamma \int_\Omega r \, (\nabla \mathbf{u})^T : \nabla \mathbf{v} \tag{71}$$

is coercive on the whole space U (and therefore in particular for $K_h \subseteq U_h \subseteq U$).

We will now prove that for $\mathbf{v}_h \in K_h$ it holds

$$\int_\Omega r \, (\nabla \mathbf{v}_h)^T : \nabla \mathbf{v}_h \geq 0 \ . \tag{72}$$

Once estimate (72) has been established, also for $\gamma < 0$ the coercivity property (62) immediately follows, and the proof is complete.

We first observe that

$$(\nabla \mathbf{v}_h)^T = (\operatorname{div} \mathbf{v}_h) \, \mathbf{I} - \operatorname{cof}[\nabla \mathbf{v}_h] \ . \tag{73}$$

Using (73) and integrating by parts we have

$$\int_\Omega r\,(\nabla \mathbf{v}_h)^T : \nabla \mathbf{v}_h = \int_\Omega r(\operatorname{div} \mathbf{v}_h)^2 - \int_\Omega r\operatorname{cof}[\nabla \mathbf{v}_h] : \nabla \mathbf{v}_h$$
$$= \int_\Omega r(\operatorname{div} \mathbf{v}_h)^2 + \int_\Omega \operatorname{div}(r\operatorname{cof}[\nabla \mathbf{v}_h]) \cdot \mathbf{v}_h \ , \tag{74}$$

where all the boundary integrals vanish because the function $r\mathbf{v}_h$ vanishes on the whole boundary $\partial\Omega$.

Due to Piola's identity and using (73) we have

$$\int_\Omega \operatorname{div}(r\operatorname{cof}[\nabla \mathbf{v}_h]) \cdot \mathbf{v}_h = \int_\Omega \operatorname{cof}[\nabla \mathbf{v}_h]\nabla r \cdot \mathbf{v}_h$$
$$= -\int_\Omega (\nabla \mathbf{v}_h)^T \nabla r \cdot \mathbf{v}_h + \int_\Omega (\operatorname{div} \mathbf{v}_h)\nabla r \cdot \mathbf{v}_h \ . \tag{75}$$

Recalling that on Γ we have $\nabla r = -\mathbf{n}$, simple algebra and an integration by parts give

$$-\int_\Omega (\nabla \mathbf{v}_h)^T \nabla r \cdot \mathbf{v}_h = -\int_\Omega \nabla r \cdot [\nabla \mathbf{v}_h]\mathbf{v}_h$$
$$= \int_\Omega (\operatorname{div} \mathbf{v}_h)\nabla r \cdot \mathbf{v}_h - \int_\Gamma (\mathbf{v}_h \cdot \mathbf{n})(\mathbf{v}_h \cdot \nabla r)$$
$$= \int_\Omega (\operatorname{div} \mathbf{v}_h)\nabla r \cdot \mathbf{v}_h + \int_\Gamma \mid \mathbf{v}_h \cdot \mathbf{n} \mid^2 \ . \tag{76}$$

Using (74), (75) and (76) it follows

$$\int_\Omega r\,(\nabla \mathbf{v}_h)^T : \nabla \mathbf{v}_h = \int_\Omega r(\operatorname{div} \mathbf{v}_h)^2 + 2\int_\Omega (\operatorname{div} \mathbf{v}_h)(\nabla r \cdot \mathbf{v}_h) + \int_\Gamma \mid \mathbf{v}_h \cdot \mathbf{n} \mid^2 \ . \tag{77}$$

We now split each component of $\mathbf{v}_h$ in its linear and bubble parts, i.e.

$$\mathbf{v}_h = \mathbf{v}_h^L + \mathbf{v}_h^B = (v_1^L + v_1^B, v_2^L + v_2^B) \ . \tag{78}$$

Accordingly, noting also that

$$\nabla r \cdot \mathbf{v}_h = -(v_2^L + v_2^B) \ , \tag{79}$$

equation (77) can be written as

$$\int_\Omega r\,(\nabla \mathbf{v}_h)^T : \nabla \mathbf{v}_h = \int_\Omega r\Big(\operatorname{div}(\mathbf{v}_h^L + \mathbf{v}_h^B)\Big)^2 - 2\int_\Omega \Big(\operatorname{div}(\mathbf{v}_h^L + \mathbf{v}_h^B)\Big)(v_2^L + v_2^B) + \int_\Gamma |\ (\mathbf{v}_h^L + \mathbf{v}_h^B)\cdot \mathbf{n}\ |^2 = A_1 + A_2 + A_3\ . \tag{80}$$

We now estimate the three terms above. We obviously have

$$A_1 := \int_\Omega r\Big(\operatorname{div}(\mathbf{v}_h^L + \mathbf{v}_h^B)\Big)^2 \geq 2\int_\Omega r(\operatorname{div}\mathbf{v}_h^L)(\operatorname{div}\mathbf{v}_h^B)\ . \tag{81}$$

Integrating by parts and using that $\nabla r \cdot \mathbf{v}_h^B = -v_2^B$, from (81) we obtain

$$A_1 \geq -2\int_\Omega (\operatorname{div}\mathbf{v}_h^L)\nabla r\cdot \mathbf{v}_h^B = 2\int_\Omega (\operatorname{div}\mathbf{v}_h^L) v_2^B\ . \tag{82}$$

Recalling that $\mathbf{v}_h = \mathbf{v}_h^L + \mathbf{v}_h^B \in K_h$ and observing that v_2^L is a continuous piecewise linear function, it follows that

$$A_2 := -2\int_\Omega \Big(\operatorname{div}(\mathbf{v}_h^L + \mathbf{v}_h^B)\Big)(v_2^L + v_2^B) = -2\int_\Omega \Big(\operatorname{div}(\mathbf{v}_h^L + \mathbf{v}_h^B)\Big) v_2^B\ . \tag{83}$$

Since it holds

$$\int_\Omega (\operatorname{div}\mathbf{v}_h^B) v_2^B = 0\ , \tag{84}$$

from (83) we get

$$A_2 = -2\int_\Omega (\operatorname{div}\mathbf{v}_h^L) v_2^B\ . \tag{85}$$

Furthermore, for A_3 we obviously have

$$A_3 := \int_\Gamma |\ (\mathbf{v}_h^L + \mathbf{v}_h^B)\cdot\mathbf{n}\ |^2 \geq 0\ . \tag{86}$$

Collecting (82),(85) and (86), we finally get (cf. (80))

$$\int_\Omega r\,(\nabla \mathbf{v}_h)^T : \nabla \mathbf{v}_h \geq 2\int_\Omega (\operatorname{div} \mathbf{v}_h^L) v_2^B - 2\int_\Omega (\operatorname{div} \mathbf{v}_h^L) v_2^B = 0\ . \qquad (87)$$

The Proposition is proved. □

4.2 The QME element

We now consider the discretized counterpart of problem (16), using the QME quadrilateral method proposed by Pantuso-Bathe (cf. [18]) and based on the *Enhanced Strain Technique* (cf. [24], for instance). This scheme optimally performs in small deformation regimes, as theoretically proved in [13].

For our analysis we consider uniform meshes $\mathcal{T}_h$ formed by equal square elements K with side length h, as the ones used in the numerical tests of Section 5.

The Pantuso-Bathe element is described by the following choice of spaces. For the discretization of the displacement field, we take

$$U_h = \left\{ \mathbf{v}_h \in U \ :\ \mathbf{v}_{h|K} \in \mathcal{Q}_1(K)^2 \qquad \forall K \in \mathcal{T}_h \right\}\ , \qquad (88)$$

where $\mathcal{Q}_1(K)$ is the standard space of bilinear functions. For the pressure discretization, we take

$$P_h = \left\{ q_h \in H^1(\Omega) \ :\ q_{h|K} \in \mathcal{Q}_1(K) \qquad \forall K \in \mathcal{T}_h \right\}\ . \qquad (89)$$

Furthermore, the *Enhanced Strain* space is described by

$$S_h = \left\{ \mathbf{E}_h \in (L^2(\Omega))^4 \ :\ \mathbf{E}_{h|K} \in E_6(K) \qquad \forall K \in \mathcal{T}_h \right\}\ . \qquad (90)$$

Above, $E_6(K)$ is the space of tensor-valued functions defined on K, spanned by the following shape functions

$$\begin{bmatrix} \alpha_1\xi + \alpha_2\xi\eta\ ; & \alpha_3\xi \\ \alpha_4\eta & ;\ \alpha_5\eta + \alpha_6\xi\eta \end{bmatrix} \qquad \text{with } \alpha_i \in \mathbf{R}\ , \qquad (91)$$

where (ξ, η) denotes the standard local coordinates on K.

Therefore, the discretization of problem (16) reads as follows.

Find $(\mathbf{u}_h, \mathbf{H}_h; p_h) \in (U_h \times S_h) \times P_h$ such that:

$$\begin{cases} 2\mu \displaystyle\int_\Omega (\nabla \mathbf{u}_h + \mathbf{H}_h)^S : (\nabla \mathbf{v}_h + \mathbf{E}_h)^S - \gamma \int_\Omega r\, (\nabla \mathbf{u}_h + \mathbf{H}_h)^T : (\nabla \mathbf{v}_h + \mathbf{E}_h) \\ \\ \quad + \displaystyle\int_\Omega p_h\, (\operatorname{div} \mathbf{v}_h + \operatorname{tr} \mathbf{E}_h) = \Delta\gamma \int_\Omega \mathbf{f} \cdot \mathbf{v}_h \qquad \forall (\mathbf{v}_h, \mathbf{E}_h) \in U_h \times S_h \\ \\ \displaystyle\int_\Omega q_h (\operatorname{div} \mathbf{u}_h + \operatorname{tr} \mathbf{H}_h) = 0 \qquad\qquad\qquad\qquad \forall q_h \in P_h\ . \end{cases} \tag{92}$$

Above and in the sequel, we denote with "tr" the trace operator acting on tensors.

Introducing the discrete kernel as

$$K_h = \left\{ (\mathbf{v}_h, \mathbf{E}_h) \in U_h \times S_h \ :\ \int_\Omega q_h (\operatorname{div} \mathbf{v}_h + \operatorname{tr} \mathbf{E}_h) = 0 \qquad \forall q_h \in P_h \right\}\ , \tag{93}$$

we are interested in analyzing for which γ there exists a constant $c_E(\gamma, \mu)$ such that (cf. (18))

$$a_\gamma(\nabla \mathbf{v}_h + \mathbf{E}_h, \nabla \mathbf{v}_h + \mathbf{E}_h) \geq c_E(\gamma, \mu) \int_\Omega \left(|\boldsymbol{\varepsilon}(\mathbf{v}_h)|^2 + |\mathbf{E}_h|^2 \right) \tag{94}$$

for every $(\mathbf{v}_h, \mathbf{E}_h) \in K_h$.

We have the following result.

Proposition 9 *For the choice (88)–(91), the discrete coercivity on the kernel condition (94) does not hold, whenever $\gamma > \mu$.*

Proof. Let us define the set $F(\gamma) \subset \Omega$ by

$$F(\gamma) = \left\{ (X, Y) \in \Omega \ :\ 2\mu - \gamma\, r(X, Y) \leq 0 \right\}\ . \tag{95}$$

Recalling that $r(X, Y) = 1 - Y$, the set $F(\gamma)$ has positive area for $\gamma > \mu$. It follows that, for sufficiently small h, there exists $\tilde{K} \in \mathcal{T}_h$ completely contained in $F(\gamma)$. Now take $(\mathbf{v}_h, \mathbf{E}_h) \in U_h \times S_h$ by choosing $\mathbf{v}_h = 0$ and $\mathbf{E}_h$ vanishing outside $\tilde{K}$. Moreover, in $\tilde{K}$ choose (cf. (91))

$$\mathbf{E}_{h|\tilde{K}} = \begin{bmatrix} \alpha\xi\eta\ ; & 0 \\ 0 & ;\ -\alpha\xi\eta \end{bmatrix} \qquad \text{with } \alpha \neq 0\ . \tag{96}$$

Notice that $\mathrm{tr}\,\mathbf{E}_h = 0$; hence $(0,0) \neq (0,\mathbf{E}_h) \in K_h$ (cf. (93)). On the other hand, a direct computation shows that

$$a_\gamma(\mathbf{E}_h,\mathbf{E}_h) = \int_{\tilde{K}} (2\mu - \gamma\, r)|\mathbf{E}_h|^2 \ . \tag{97}$$

Since $\tilde{K} \subseteq F(\gamma)$, we have $(2\mu - \gamma\, r) \leq 0$, so that (97) implies

$$a_\gamma(\mathbf{E}_h,\mathbf{E}_h) \leq 0 \ . \tag{98}$$

As a consequence the form $a_\gamma(\cdot,\cdot)$ cannot be coercive on K_h for $\gamma > \mu$, uniformly in h. $\square$

5 Numerical tests

We now study the computational performances of specific finite element interpolations on the model problem presented in Section 3. In particular, we wish to numerically detect the stability range of the elements under investigation and compare such numerical results with the theoretical ones obtained for the *discrete* problems in Sections 4.1-4.2 and for the *continuous* problem in Section 3.

Besides the interpolations discussed in Sections 4.1 and 4.2, for the numerical investigation we also consider the so-called Q2P1 (see, for instance, [9]), since this is commonly considered as a very stable element. Accordingly, we deal with the following interpolation schemes:

- MINI – Triangular element with piecewise linear continuous approximation for both the displacements and the pressure, with the displacements enriched by a cubic bubble as proposed in [1].
- QME – Quadrilateral element with piecewise bilinear continuous approximation for both the displacements and the pressure, enriched by the Enhanced Strains as proposed in [18].
- Q2P1 – Quadrilateral element with piecewise biquadratic continuous approximation for the displacements and piecewise linear approximation for the pressure.

All the schemes have been implemented in FEAP (see [25]). The model problem is sketched in Fig. 1, and, assuming to express respectively forces and lengths in KN and m, we set $\mu = 40$ and $\mathbf{f} = (0,\gamma)^T$, where γ plays the role of load multiplier. In particular, we find convenient to express the numerical results in terms of the nondimensional quantity $\tilde{\gamma}$ defined as $\tilde{\gamma} = \gamma L/\mu$

with L some problem characteristic length, in the following set equal to 1 for simplicity and consistently with the model problem.

For a given interpolation scheme and for a given mesh, to detect numerically the element stability range we progressively increase the load multiplier γ, adopting an iterative Newton-Raphson scheme to obtain the solution corresponding to the single load value from the solution corresponding to the previous load value. In particular, we increase the load multiplier by a quantity $\Delta\gamma$ until some form of numerical instabilities appears; we indicate the load multiplier corresponding to the appearance of numerical instabilities with γ_{cr} with the corresponding nondimensional multiplier as $\tilde{\gamma}_{cr}$. To investigate very large load multiplier intervals, we adopt different increments $\Delta\gamma$ depending on the load level (Table 1).

Clearly, the analyses are performed starting from $\tilde{\gamma} = 0$ for both positive and negative loading conditions, i.e. for $\tilde{\gamma} < 0$ and $\tilde{\gamma} > 0$. Finally, if we do not detect numerical instabilities even for extremely large values of the load multiplier ($\tilde{\gamma} > 10^6$) we set $\tilde{\gamma}_{cr} = \infty$.

Tables 2, 3 and 4 report the stability limits for the different interpolation schemes considered. From the tables we may make the following observations.

- The theoretical predictions for the MINI interpolation scheme are that the *discrete* problem is stable for $-\infty < \tilde{\gamma} < 1$ and unstable for $\tilde{\gamma} > 3/2$ (cf. Propositions 7 and 8). The results presented in Table 2 show that the corresponding *numerical* problem is stable for $-\infty < \tilde{\gamma} < 1$, unstable for $\tilde{\gamma} > 3/2$. In particular, the stability upper limit approaches monotonically 1 from above during the mesh refinement (i.e. for $h \to 0$). Accordingly, for the MINI interpolation scheme the numerical results presented in Table 2 confirm the theoretical predictions.
- The theoretical predictions for the QME interpolation scheme are that for sufficiently small h the *discrete* problem is unstable for $\tilde{\gamma} > 1$ (cf. Proposition 8). The results presented in Table 3 seem to indicate that for sufficiently small h the corresponding *numerical* problem is stable for $-\infty < \tilde{\gamma} < 1$ and unstable for $\tilde{\gamma} > 1$. In particular, the stability lower limit is decreasing almost linearly with h, approaching $-\infty$ for $h \to 0$, while the stability upper limit is about 1 but it does not seem to have a smooth convergence. Accordingly, also for the QME interpolation scheme the numerical results presented in Table 3 confirm the theoretical predictions.
- We do not have theoretical prediction for the Q2P1 *discrete* problem, except the trivial one telling that the problem is stable in the range $-1 < \tilde{\gamma} < 1$ (cf. the proof of Proposition 8, at the beginning). However, the results presented in Table 4 and relative to the Q2P1 interpolation scheme seem to indicate that independently of h the *numerical* problem is stable for $-\infty < \tilde{\gamma} < \infty$. However, we note that during the analyses the finite element code FEAP

$\Delta\gamma = 10^{-1}$	up to	$\gamma = 10^2$
$\Delta\gamma = 1$	up to	$\gamma = 10^3$
$\Delta\gamma = 10$	up to	$\gamma = 10^4$
$\Delta\gamma = 10^2$	up to	$\gamma = 10^5$
$\Delta\gamma = 10^3$	up to	$\gamma = 10^6$

Table 1
Load increments $\Delta\gamma$ (depending on the load level γ) for the Newton-Raphson scheme.

mesh	$\tilde{\gamma}_{cr}^{-}$	$\tilde{\gamma}_{cr}^{+}$
4×4	$-\infty$	1.28
8×8	$-\infty$	1.22
16×16	$-\infty$	1.19
32×32	$-\infty$	1.18
64×64	$-\infty$	1.17
128×128	$-\infty$	1.12

Table 2
MINI element: numerical stability limits for the model problem.

gives a warning about a change in the stiffness matrix properties for $\tilde{\gamma}$ approximatively in the range $[1, 3/2]$. We believe that this point could be of interest, however it requires further investigations.

Finally, we recall that the *continuous* problem is stable at least for $-\infty < \tilde{\gamma} < 3$ (see (56)), and that for a sufficiently large value of $\tilde{\gamma}$ the problem gets unstable (see Remark 4). Therefore, we may conclude that all the interpolation schemes fail in properly detecting the stability range of the continuous problem. In particular, the MINI interpolation scheme seems to be the most effective in the sense that it is the element able to reproduce more closely (but still in a deficient form) the continuum problem; the QME interpolation scheme seems to be too "flexible" while the Q2P1 seems to be too "stiff".

6 Conclusions

We have proposed a simple 2D finite-strain problem depending on a loading parameter, for which a trivial solution can be easily computed. We have proved the stability of such a solution whenever the loading parameter stays in a suitable range of values. Furthermore, we have considered and analyzed the problem discretization by means of some mixed finite elements, which are

mesh	$\tilde{\gamma}_{cr}^{-}$	$\tilde{\gamma}_{cr}^{+}$
4×4	-52.8	1.21
8×8	-150	1.07
16×16	-335	0.998
32×32	-723	0.978
64×64	-1480	0.980
128×128	-2980	0.983

Table 3
QME element: numerical stability limits for the model problem.

mesh	$\tilde{\gamma}_{cr}^{-}$	$\tilde{\gamma}_{cr}^{+}$
4×4	$-\infty$	$+\infty$
8×8	$-\infty$	$+\infty$
16×16	$-\infty$	$+\infty$
32×32	$-\infty$	$+\infty$
64×64	$-\infty$	$+\infty$
128×128	$-\infty$	$+\infty$

Table 4
Q2P1 element: numerical stability limits for the model problem.

known to optimally behave in the framework of small deformation problems. In particular, we have proved that the elements fail to properly detect the problem stability range. We have also presented several numerical experiments, in accordance with the theoretical predictions. We conclude by noting that our analysis is not able to *fully* explain the numerical behavior of the schemes under investigation, and some points need to be better studied and clarified. This will be the topic of future communications.

Acknowledgments

The authors would like to thank Prof. T.J.R. Hughes, University of Texas at Austin, for the very valuable discussions on the subject of this paper.

This work has been partially supported by the European Project HPRN-CT-2002-00284 "New Materials, Adaptive Systems and their Nonlinearities. Modelling, Control and Numerical Simulation".

References

[1] Arnold DN, Brezzi F, Fortin M. A stable finite element for the Stokes equation, Calcolo 1984; 21:337-344.

[2] Auricchio F, Beirão da Veiga L, Lovadina C, Reali A. Triangular Enhanced Strain Elements for Plane Linear Elasticity, submitted to Comput. Meth. Appl. Mech. Engrg.

[3] Armero F. On the locking and stability of finite elements in finite deformation plane strain problems. Computers and Structures 2000; 75:261-290.

[4] Bathe KJ. Finite Element Procedures, Prentice Hall, Englewood Cliffs, NJ, 1996.

[5] Braess D. Enhanced assumed strain elements and locking in membrane problems. Comput. Meth. Appl. Mech. Engrg. 1998; 165:155-174.

[6] Bonet J, Wood R.D. Nonlinear continuum mechanics for finite element analysis. Cambridge University Press, 1997

[7] Brezzi F, Fortin M. Mixed and hybrid Finite Element Methods, Springer-Verlag, New York, 1991.

[8] Ciarlet PG. Mathematical Elasticity. Volume 1: Three dimensional elasticity. North-Holland, Amsterdam, 1998.

[9] Hughes TJR. The Finite Element Method. Dover Publications, NY, 2000.

[10] Klaas O, Maniatty AM, Shephard. MS A Stabilized Mixed Petrov-Galerkin Finite Element Method for Finite Elasticity. Formulation for Linear Displacement and Pressure Interpolation. Comput Methods Appl. Mech. Engrg. 1999; 180:65-79.

[11] Le Tallec P. Existence and approximation results for nonlinear mixed problems: application to incompressible finite elasticity. Numer. Math. 1982; 38:365-382.

[12] Le Tallec P. Numerical Methods for nonlinear three-dimensional elasticity. In: Handbook of numerical analysis, Vol III 1994; 465-622.

[13] Lovadina C. Analysis of strain-pressure finite element methods for the Stokes problem. Numer. Methods for PDE's 1997; 13:717-730.

[14] Lovadina C, Auricchio F. On the Enhanced Strain Technique for Elasticity Problems. Computers and Structures, 2003; 81:777-787.

[15] Maniatty AM, Liu Y, Klaas O, Shephard MS. Higher Order Stabilized Finite Element Method for Hyperelastic Finite Deformation. Comput Methods Appl. Mech. Engrg. 2002; 191:1491-1503.

[16] Marsden JE, Hughes TJR. Mathematical Foundations of Elasticity. Dover Publications, NY, 1993.

[17] Nagtegaal JC, Fox DD. Using assumed enhanced strain elements for large compressive deformation. Int. J. Solids Structures 1996; 33:3151-3159.

[18] Pantuso D, Bathe KJ. A four-node quadrilateral mixed-interpolated element for solids and fluids. Math. Models Methods Appl. Sci. 1995; 5:1113-1128.

[19] Pantuso D, Bathe KJ. On the stability of mixed finite elements in large strain analysis of incompressible solids. Finite Elements in Analysis and Design 1997; 28:83-104.

[20] Reddy BD, Simo JC. Stability and convergence of a class of enhanced strain methods. SIAM J. Numer. Anal. 1995; 32(6):1705-1728.

[21] Reese S, Küssner M, Reddy BD. A new stabilization technique for finite elements in non-linear elasticity. Int. J. Numer. Meth. Engng. 1999; 44:1617-1652.

[22] Reese S, Wriggers P. A stabilization technique to avoid hourglassing in finite elasticity. Int. J. Numer. Meth. Engng. 2000; 48:79-109.

[23] Simo JC, Armero F. Geometrically nonlinear enhanced strain mixed methods and the method of incompatible modes. Int. J. Numer. Meth. Engng. 1992; 33:1413-1449.

[24] Simo JC, Rifai MS. A class of mixed assumed strain methods and the method of incompatible modes. Int. J. Numer. Meth. Engng. 1990; 29:1595-1638.

[25] Taylor RL. FEAP: A Finite Element Analysis Program, Programmer Manual, (`http://www.ce.berkeley.edu/~rlt/feap/`).

[26] Wriggers P, Reese S. A note on enhanced strain methods for large deformations. Comput. Methods Appl. Mech. Engrg. 1996; 135:201-209.